Simultaneous Wind and Rain Retrieval Using SeaWinds Data

David W. Draper and David G. Long, *Senior Member, IEEE*

***Abstract*—The SeaWinds scatterometers onboard the QuikSCAT and the Advanced Earth Observing Satellite 2 measure ocean winds on a global scale via the relationship between the normalized radar backscattering cross section of the ocean and the vector wind. The current wind retrieval method ignores scattering and attenuation of ocean rain, which alter backscatter measurements and corrupt retrieved winds. Using a simple rain backscatter and attenuation model, two methods of improving wind estimation in the presence of rain are evaluated. First, if no suitable prior knowledge of the rain rate is available, a maximum-likelihood estimation technique is used to simultaneously retrieve the wind velocity and rain rate. Second, when a suitable outside estimate of the rain rate is available, wind retrieval is performed by correcting the wind geophysical model function for the known rain via the rain backscatter model. The new retrieval techniques are evaluated via simulation and validation with data from the National Centers for Environmental Prediction and the Tropical Rainfall Measuring Mission Precipitation Radar. The simultaneous wind/rain estimation method yields most accurate winds in the "sweet spot" of SeaWinds' swath. On the outer-beam edges of the swath, simultaneous wind/rain estimation is not usable. Wind speeds from simultaneous wind/rain retrieval are nearly unbiased for all rain rates and wind speeds, while conventionally retrieved wind speeds become increasingly biased with rain rate. A synoptic example demonstrates that the new method is capable of reducing the rain-induced wind vector error while producing a consistent (yet noisy) estimate of the rain rate.**

***Index Terms*—Maximum-likelihood, scatterometer, SeaWinds, simultaneous wind/rain retrieval, Tropical Rainfall Measuring Mission (TRMM) Precipitation Radar (PR).**

I. Introduction

THE SEAWINDS scatterometers aboard QuikSCAT, launched in mid 1999, and the Advanced Earth Observing Satellite 2 (ADEOS II), launched in November 2002 by the National Aeronautics and Space Administration (NASA), provide a unique and valuable source for widespread observation of near-surface ocean winds. The SeaWinds rotating pencil beam design enables wider coverage than previous fan-beam instruments like the NASA Scatterometer (NSCAT) [1]. Validation studies demonstrate that the SeaWinds scatterometer operates at high accuracy in most wind and weather conditions, e.g., see [2] and [3].

SeaWinds scatterometer wind estimation is possible due to the relationship between the near-surface vector wind and the normalized radar backscattering cross section (σ°) of the ocean surface [4], [5]. This relationship has been empirically determined and is known as the geophysical model function (GMF) [6]–[8]. The GMF is a function of wind speed, wind direction relative to the antenna azimuth angle, incidence angle, polarization, and frequency. Wind estimates are formed by inverting the GMF given several σ° measurements from different azimuth angles [9].

During rain (which affects about 4% of SeaWinds data), the scatterometer σ° measurements are augmented by additional backscatter from both atmospheric rain and surface rain perturbations [10]–[13]. The returned signal from the wind-roughened seas is also attenuated by falling hydrometeors. A simple empirical rain backscatter and attenuation model for use with SeaWinds is developed and evaluated in [14]. Because the GMF does not account for rain affects, the additional scattering from rain causes estimated wind speeds to appear higher than expected. Also, the directions of rain-corrupted wind vectors generally point cross swath, regardless of the true wind [15].

The degradation of SeaWinds on QuikSCAT scatterometer accuracy during rain prompted development of a probability-based rain flag given several rain-sensitive parameters, known as the multidimensional histogram (MUDH) rain flag [15]. Besides the MUDH flag, a variety of other rain flags for SeaWinds on QuikSCAT have been suggested, e.g., [16]–[19], but no formal attempt has been made to correct rain-corrupted wind vectors.

This paper discusses a novel method for improving wind estimates in the presence of rain using the simple rain-backscatter model developed in [14]. The paper focuses on two wind retrieval methods: simultaneous wind/rain estimation and rain-corrected wind retrieval. First, when an estimate of the rain rate is not available, the wind velocity and rain rate is simultaneously retrieved using maximum-likelihood estimation (MLE). This method can be used for postcorrection of SeaWinds on QuikSCAT data, and to provide an auxiliary earthwide database of rain rates. Second, when knowledge of the rain rate is available, the GMF is directly corrected for the known rain rate. The wind is then retrieved using the adjusted GMF. The rain-corrected retrieval technique can be used to provide a more accurate wind estimate than simultaneous wind/rain retrieval by eliminating rain rate ambiguity.

After presenting background on the conventional wind retrieval method in Section II, this paper describes the combined wind/rain MLE approaches in Section III. In conjunction with SeaWinds rain retrieval, wind vector cell filling variability is discussed in Section III-C, along with a calculation of the normalized standard deviation of the rain backscatter model in Sec-

Manuscript received December 22, 2003; revised April 9, 2004.

D. W. Draper was with the Microwave Earth Remote Sensing Laboratory, Brigham Young University, Provo, UT 84602 USA. He is now with Ball Aerospace, Boulder, CO 80301 USA.

D. G. Long is with the Microwave Earth Remote Sensing Laboratory, Brigham Young University, Provo, UT 84602 USA (e-mail: long@byu.edu).

Digital Object Identifier 10.1109/TGRS.2004.830169

tion V. The paper evaluates the wind retrieval skill for both simultaneous wind/rain and rain-corrected methods via simulation, comparing each method to the conventional wind-only retrieval in Section VI.

In addition, validation studies are performed for the MLE approach with colocated data from the Tropical Rainfall Measuring Mission (TRMM) Precipitation Radar (PR), and winds from the National Centers for Environmental Prediction (NCEP). These data are used to train the model and are described in detail [14]. The comparison dataset contains 100 disjoint sections of the TRMM PR swath over a three-month period, from August to October 1999. The data are colocated spatially and temporally with QuikSCAT to within 10 min and only include regions in which overlapping TRMM PR swath has more than 2.5% measurements flagged as "rain certain." Thus, only regions with significant amount of rain contamination are used. Due to the orbit of TRMM, the colocated set restricted to a latitude band within $\pm 37^\circ$ of the equator. For wind retrieval validation of the simultaneous wind/rain technique, NCEP 1000-mbar winds from the QuikSCAT L2B dataset are used. These wind data are trilinearly interpolated (in space and time) from a $2.5^\circ \times 2.5^\circ$ latitude-longitude grid with a temporal resolution of 6 h. A bias correction, valid over the colocated dataset, is applied to the NCEP winds to adjust for differences in reference height. The colocated set contains approximately 250 000 QuikSCAT wind vector cells, approximately half of which contain some rain within the footprint. The set is large enough to contain a representative sample of wind speeds over the tropics, and a large range of rain rates. Additional validation against radiometer data is given in the companion paper [20].

A synoptic example is given in Section VII, demonstrating the utility of simultaneous wind/rain retrieval. Simulation and validation demonstrate that the simultaneous wind/rain retrieval method works best in the swath sweet spot, and is not usable on the swath edges. As expected, the nadir region tends to be noisier than the sweet spot. The method works well for most wind and rain conditions, although some wind/rain states cause ambiguity between wind speed and rain rate, resulting in spurious rain rate estimates or abnormally low wind speed estimates. Such anomalies usually occur in extreme wind or rain conditions, and in connection with cross-swath blowing winds. In zero-rain conditions, simultaneous wind/rain retrieval produces somewhat noisier results than the conventional method, especially at nadir. Further work is intended for quality control in such areas of degraded performance.

II. Data

This section provides a brief background of wind scatterometry and a description of the SeaWinds instrument. The main backscattering mechanism at scatterometer incidence angles is Bragg resonance from waves on the order of the electromagnetic wavelength [5] (a few centimeters for SeaWinds). The amplitude of the centimeter-scale capillary waves are in large part driven by wind stress on the surface of the water [21]. Ocean backscatter is a function of the magnitude and orientation of the waves, and is thus a function of the vector wind stress. Given neutral stability conditions (equal surface air and surface temperature with an adiabatic lapse rate), the backscatter is also related to the wind at a given reference height (traditionally 10 or 19.5 m) [22]. The relationship between the neutral stability wind velocity and σ° is described by the GMF.

Because the GMF maps two parameters (speed and direction) to one (σ°), retrieving both wind speed and direction over the ocean requires multiple σ° measurements from various azimuth angles [23]. The SeaWinds antenna is designed with two offset-fed beams: an inner h-polarization beam at an incidence angle of approximately 46°, and an outer v-polarization beam at an incidence angle of 54°. The SeaWinds rotating antenna design achieves the needed azimuthal diversity by measuring each point on the surface at least four times, twice by each beam (fore and aft) as the antenna rotates [1]. In standard SeaWinds processing, the satellite swath is segmented into approximately 25 km × 25 km wind vector cells (WVCs). The σ° measurements with centers located within the 25×25 km WVC are used to create a wind vector estimate at that WVC. The SeaWinds design affords a wide 1800-km swath (72 WVCs in the cross-track direction), covering 90% of the earth on a daily basis.

Due to the scanning pencil beam design, measurement geometry varies along the cross track. In the center of the swath (nadir region), the fore and aft beams are nearly 180°apart, while the difference in azimuth between fore and aft beams goes to zero on the swath edges. Also, the outer nine WVCs on either side of the swath only obtain measurements from the outer v-polarization beam. Thus, the outer-beam swath edges and the nadir region have a somewhat poor viewing geometry for wind estimation. In the off-nadir inner-beam regions, known as the "sweet spots," the azimuthal diversity is very well suited for wind retrieval [24].

Estimating wind speed and direction involves inverting the GMF given colocated σ° measurements at each WVC. The GMF inversion method adopted for SeaWinds is a MLE technique [9]. Assuming Gaussian noise and independent samples, the probability of the σ° measurements given the surface wind velocity is

$$p(\mathbf{z}|\mathbf{u}) = \prod_k \frac{1}{\sqrt{2\pi}\varsigma_k} \exp\left\{-\frac{1}{2}\frac{(z_k - \mathcal{M}(\mathbf{u}, \phi_k, \ldots))^2}{\varsigma_k^2}\right\} \quad (1)$$

where $\mathbf{z}$ is a vector containing the measured σ° values, ς_k^2 is the measurement variance, $\mathcal{M}$ is the GMF, $\mathbf{u} = \{u, d\}$ is the wind speed and direction, and ϕ_k the azimuth angle of the instrument.

The mean corresponding to the probability distribution given in (1) is the GMF σ° values given the true wind speed and direction. The variance is a combination of uncertainty in the GMF, signal noise due to fading, and thermal noise. Traditionally, the variance is defined in terms of K_{pm}, the normalized standard deviation of the GMF, and K_{pc}, the normalized standard deviation of the communication or signal noise. The total variance of σ° is given by [25]

$$\varsigma^2(\mathbf{u}) = (K_{pc}^2 + K_{pm}^2 + K_{pc}^2 K_{pm}^2)\mathcal{M}^2(\mathbf{u}) \quad (2)$$

where K_{pc} is generally written as

$$K_{pc} = \sqrt{\alpha + \frac{\beta}{\sigma_t} + \frac{\gamma}{\sigma_t^2}}. \quad (3)$$

The coefficients α, β, and γ depend on fading characteristics of the surface scatterers and the SNR at the receiver [24], [26]. σ_t is the true σ° without communication noise.

For SeaWinds processing, K_{pm} is assumed to be constant, and σ_t is approximated by the model function estimate of σ°

$$\sigma_t \cong \mathcal{M}(\mathbf{u}). \tag{4}$$

Using this approximation, and combining (2) and (3) yields

$$\varsigma^2(\mathbf{u}) \cong \alpha\mathcal{M}(\mathbf{u})^2 + \beta\mathcal{M}(\mathbf{u}) + \gamma + K_{pm}^2\left[(1+\alpha)\mathcal{M}(\mathbf{u})^2 + \beta\mathcal{M}(\mathbf{u}) + \gamma\right]. \tag{5}$$

SeaWinds processing simplifies (5) by the assumption

$$(1+\alpha)\mathcal{M}(\mathbf{u})^2 \gg \beta\mathcal{M}(\mathbf{u}) + \gamma \tag{6}$$

yielding (after some algebra)

$$\varsigma^2(\mathbf{u}) \cong [(1+\alpha)K_{pm}^2 + \alpha]\mathcal{M}^2(\mathbf{u}) + \beta\mathcal{M}(\mathbf{u}) + \gamma. \tag{7}$$

The coefficients $\mathrm{kp\_alpha} = (1+\alpha)$, $\mathrm{kp\_beta} = \beta$, and $\mathrm{kp\_gamma} = \gamma$ are computed and stored in the standard SeaWinds L2A product.

The SeaWinds data processor estimates the wind via the simplified likelihood function formed by treating the outside variance term of (1) as a constant, taking the negative logarithm, and dropping constant terms [25], yielding

$$l(\mathbf{z}|\mathbf{u}) = \sum_k \frac{(z_k - \mathcal{M}_k(\mathbf{u},\ldots))^2}{\varsigma_k(\mathbf{u})^2}. \tag{8}$$

An iterative search routine is applied to find the maxima of (8), in which the variance term is computed from each trial wind vector. Because of symmetry in the GMF and uncertainty from noise, the likelihood function generally has 1 to 4 local minima, each representing a possible wind vector solution. The wind vectors corresponding to the local minima are known as ambiguities.

After generating the set of ambiguities at each WVC, an ambiguity selection routine is required to produce a unique wind vector field. The traditional ambiguity selection approach involves two steps: nudging and median filtering. Nudging sets each WVC to the ambiguity closest to an outside estimate of the wind. The NASA Jet Propulsion Laboratory (JPL) uses numerical weather prediction (NWP) winds from the National Centers for Environmental Prediction (NCEP) as the nudging wind field. For SeaWinds on QuikSCAT, JPL implements a variant of nudging known as thresholded nudging [27]. In thresholded nudging, the set of ambiguities used in nudging depends on the likelihood values of the ambiguities. Only the ambiguities whose likelihood values are sufficiently close to the minimum value are used. After nudging, the median filter step iteratively selects the ambiguity at each WVC that most closely matches the flow of the surrounding selected wind. The median filter is repeated until convergence is reached [28].

III. Methodology

The wind estimation process described in Section II assumes that the effects from unmodeled factors such as salinity, sea and air temperature, sea foam, and rain are small. The GMF variance term K_{pm} helps account for small perturbations due to these unknowns in the estimation process. Rain effects, however, have been shown to be appreciable and at times dominating [14], [29].

The effect of rain on σ° can be parameterized by the additional scattering and attenuation of the signal

$$\sigma_m = \sigma_{\mathrm{w}}\alpha_r + \sigma_e \tag{9}$$

where σ_m is the measured backscatter, σ_{w} is the component of the backscatter due to wind, α_r is the two-way atmospheric attenuation from falling rain, and σ_e is the effective rain backscatter due to surface perturbations and atmospheric scattering [14], [29], [30]. The parameters α_r and σ_e are assumed to be independent of azimuth angle and wind velocity, and thus solely a function of the vertically integrated rain rate in kilometers millimeters per hour. Here, we adopt the empirically derived quadratic log-log model for α_r and σ_e given in [14] for use with simultaneous wind/rain retrieval.

The simple rain-σ° model of (9) can be used in conjunction with the GMF to create a combined rain/wind model function of the form

$$\mathcal{M}_r(\mathbf{u}, R, \ldots) = \mathcal{M}(\mathbf{u},\ldots)\alpha_r(R) + \sigma_e(R) \tag{10}$$

where R is the integrated rain rate and $\mathcal{M}_r$ is the combined wind/rain model function. When R is unknown, (10) can be used to simultaneously retrieve the wind and rain. If R is known for each measurement, (10) can be used to directly correct the model values in the wind estimation process. The measurement model for the combined wind/rain case is derived in Section III-A, and the simultaneous wind/rain and rain-corrected wind retrieval methods are described in Sections III-B and III-C, respectively.

A. Wind/Rain Measurement Model

Applying an MLE technique to simultaneous wind/rain retrieval requires a measurement model for the signal and noise in the combined wind and rain signal. In the measurement model, the noise in the measurement is assumed to be white Gaussian like the nonraining case. Also, the communication noise coefficients α, β, and γ used in the conventional wind-only case are assumed to not change under raining conditions.

We assume that the wind model uncertainty and uncertainty in the rain model are independent. Given the true wind and rain, the true backscatter σ_t can be written as

$$\sigma_t = \mathcal{M}(1+\eta_1 K_{pm})10^{-\alpha_{\mathrm{dB}}(1+\eta_2 K_{pa})/10} + \sigma_e(1+\eta_3 K_{pe}) \tag{11}$$

where η_1, η_2, and η_3 are zero-mean Gaussian random variables, K_{pa} is the normalized standard deviation of α_{dB} (the model attenuation α_r in decibels), and K_{pe} is the normalized standard deviation of model effective rain backscatter. The nonlinear nature of the attenuation term introduces difficulty in calculating the overall variance of the model. Assuming that the attenuation is not very large, the attenuation term can be simplified by

truncating the Taylor's series expansion of 10^x about $x = 0$, yielding

$$\begin{aligned} 10^{-\alpha_{\rm dB}(1+\eta_2 K_{pa})/10} &= 10^{-\alpha_{dB}/10} 10^{(-\alpha_{dB}\eta_2 K_{pa}/10)} \\ &= \alpha_r 10^{(-\alpha_{dB}\eta_2 K_{pa}/10)} \\ &\cong \alpha_r(1 - \ln(\alpha_r) K_{pa}\eta_2). \end{aligned} \tag{12}$$

Further, by truncating the Taylor's series expansion of $\ln(x)$ about $x = 1$, we arrive at

$$10^{-\alpha_{\rm dB}(1+\eta_2 K_{pa})/10} \cong \alpha_r(1 + (1 - \alpha_r) K_{pa}\eta_2). \tag{13}$$

Using this approximation, the expected value of σ_t is easily calculated, giving the model equation

$$E\{\sigma_t\} = \mathcal{M}\alpha_r + \sigma_e = \mathcal{M}_r. \tag{14}$$

The variance of σ_t is also calculated using the approximation of (13), yielding

$$\mathrm{Var}\{\sigma_t\} \cong \mathcal{M}^2\alpha_r^2[K_{pm}^2 + K_{pa}^2(1-\alpha_r)^2(1+K_{pm}^2)] + \sigma_e^2 K_{pe}^2. \tag{15}$$

For low to moderate rain rates, α_r is nearly unity, making the K_{pa} term of (15) negligible. At high rain rates α_r is small, and the K_{pe} term dominates. Thus, the variability due to attenuation can be ignored, reducing the variance to

$$\mathrm{Var}\{\sigma_t\} \cong \mathcal{M}^2\alpha_r^2 K_{pm}^2 + \sigma_e^2 K_{pe}^2. \tag{16}$$

Simulations of the model variance for different values of K_{pa} support the argument that the variability of the attenuation is negligible in wind retrieval [31].

Adding communication noise, the scatterometer measurement z is modeled as

$$\begin{aligned} z &= \sigma_t(1 + K_{pc}\eta_4) \\ &\cong [\mathcal{M}\alpha_r(1+\eta_1 K_{pm}) + \sigma_e(1+\eta_3 K_{pe})](1+K_{pc}\eta_4). \end{aligned} \tag{17}$$

Using this model, the expected value of z is

$$E\{z\} = \mathcal{M}\alpha_r + \sigma_e = \mathcal{M}_r \tag{18}$$

and the variance is [31]

$$\begin{aligned} \mathrm{Var}\{z\} = (\mathcal{M}^2\alpha_r^2 K_{pm}^2 + \sigma_e^2 K_{pe}^2)(1 + K_{pc}^2) \\ + K_{pc}^2(\mathcal{M}\alpha_r + \sigma_e)^2. \end{aligned} \tag{19}$$

As in the nonraining derivation of the variance, we replace σ_t with its mean from (14). Using K_{pc} from (3), and making the assumption [similar to (6)]

$$1 + \alpha \gg \frac{\beta}{\sigma_t} + \frac{\gamma}{\sigma_t^2}. \tag{20}$$

Equation (19) becomes

$$\begin{aligned} \mathrm{Var}\{z\} = (\mathcal{M}^2\alpha_r^2 K_{pm}^2 + \sigma_e^2 K_{pe}^2)(1 + \alpha) \\ + \alpha\mathcal{M}_r^2 + \beta\mathcal{M}_r + \gamma. \end{aligned} \tag{21}$$

For zero-rain conditions, $\alpha_r \to 1$, $\sigma_e \to 0$, and $\mathcal{M}_r \to \mathcal{M}$, reducing (21) to the nonraining variance of (7).

To further simplify the variance, the first term on the right-hand side of (21) is manipulated by completing the square to yield

$$\begin{aligned} \mathrm{Var}\{z\} = [(\mathcal{M}\alpha_r K_{pm} + \sigma_e K_{pe})^2 - 2K_{pm}K_{pe}\mathcal{M}\alpha_r\sigma_e](1+\alpha) \\ + \alpha\mathcal{M}_r^2 + \beta\mathcal{M}_r + \gamma. \end{aligned} \tag{22}$$

Given that the total model backscatter $\mathcal{M}_r$ is a constant, the negative cross term in (22) is parabolic in σ_e, of the form

$$-2K_{pm}K_{pe}(\mathcal{M}_r - \sigma_e)\sigma_e \tag{23}$$

which has a minimum of $-.5K_{pm}K_{pe}$ at $\sigma_e = \mathcal{M}_r/2$. Although this negative cross term is not negligible, the parabolic nature has an adverse effect on the MLE by lowering the variance of potential estimates where the raining backscatter is on the order of half the total backscatter. The parabolic nature also raises the likelihood function, artificially discouraging estimation of rain rates in this regime. In order to eliminate this problem, we present a reduced version of the variance which eliminates the negative cross term

$$\mathrm{Var}\{z\} \cong (\mathcal{M}\alpha_r K_{pm} + \sigma_e K_{pe})^2(1+\alpha) + \alpha\mathcal{M}_r^2 + \beta\mathcal{M}_r + \gamma. \tag{24}$$

To validate this simplification, wind retrieval skill using both (21) and (24) is compared in Section V, demonstrating that (24) yields better wind speed retrieval. It is interesting to note that if $K_{pe} = K_{pm}$, the form of (24) reduces to the form of the nonraining variance as intuition suggests

$$\mathrm{Var}\{z\} \cong [(1+\alpha)K_{pm}^2 + \alpha]\mathcal{M}_r^2 + \beta\mathcal{M}_r + \gamma. \tag{25}$$

B. Simultaneous Wind/Rain Retrieval

The approximate MLE likelihood function for simultaneous wind/rain retrieval is written as

$$l_r(z|\mathbf{u}, R) = \sum_k \frac{(z_k - \mathcal{M}_{rk}(\mathbf{u}, R, \ldots))^2}{\varsigma_{rk}(\mathbf{u}, R)^2} \tag{26}$$

where $\varsigma_{rk}(\mathbf{u}, R) = \mathrm{Var}\{z\}$ is the variance derived in the previous section. Simultaneous wind and rain estimates are found by minimizing the likelihood function for $\mathbf{u}$ and R given the backscatter measurements.

As in the nonraining case, the likelihood function has several local minima corresponding to possible ambiguities. Each ambiguity has a corresponding wind speed, wind direction, and rain rate. To yield a unique wind vector field, ambiguity selection is performed. In order to follow the conventional wind-only retrieval method as much as possible, a nudging/median filtering ambiguity selection scheme is implemented. For simplicity, nudging for the simultaneous rain/wind retrieval is not thresholded as with the JPL product [27]; all ambiguities are used. Median filtering is performed using the modified vector-median filter described in [28].

C. Rain-Corrected Wind Retrieval

In the case of known rain rate, such as from the Advanced Microwave Scanning Radiometer (AMSR) on ADEOS II, simultaneous wind/rain retrieval is simplified by evaluating the

MLE likelihood function of (26) at the known rain rate only. This technique is known as rain-corrected wind retrieval and is equivalent to a Bayesian estimation technique using a delta-distributed rain rate prior. In the case of synergistic use of AMSR radiometer rain rates from ADEOS II, a realistic Bayesian prior given the AMSR rain rates may also be developed. Simultaneous wind/rain retrieval and rain-corrected retrieval are evaluated in Section VI.

IV. Wind Vector Cell Filling

Because of the relatively high spatial variability of rain, beamfilling and WVC-filling effects are significant factors in interpreting SeaWinds-retrieved rain rates. The retrieved rain rate corresponding to the selected local minimum of the likelihood function is an irregularly weighted average over an area larger than the 25×25 km WVC. For each measurement, the antenna beam response function weights the backscatter values received from the atmospheric and surface rain scatterers. Thus, depending on the spatial distribution of the rain within the footprint, the backscatter response is altered from the true unweighted average. This is known as the beamfilling effect. The variability due to beamfilling is evaluated in [14]. In general, beamfilling for individual measurements introduces variability with a normalized standard deviation of 0.21. Additionally, the spatial layout of the σ° measurements within a WVC, with the associated overlap and possible lack of coverage, yields an irregularly weighted rain rate estimate. This is the WVC-filling effect.

To evaluate the WVC-filling effect, we use the TRMM PR/QuikSCAT colocated data described in the introduction. The TRMM PR obtains measurements at a much higher resolution than the SeaWinds scatterometer (about 4 km), affording an excellent dataset for analysis of subpixel spatial variability.

We examine the WVC-filling effect by evaluating the error between the "effective" weighted average rain rate seen by SeaWinds and the nonweighted rain rate averaged over each 25×25 km WVC. The weighted average rain rate $R_{\mathrm{w}}^{\mathrm{wvc}}$ is calculated by first computing the PR-derived antenna-weighted rain rate for each measurement in the colocated TRMM/SeaWinds dataset, given by

$$R_{\mathrm{w}} = \frac{\sum_{i=1}^{N} G_i R'_{\mathrm{i(PR)}}}{\sum_{i=1}^{N} G_i} \tag{27}$$

where G_i is the gain of the SeaWinds antenna pattern at each colocated TRMM PR measurement within the 6-dB SeaWinds footprint, $R'_{\mathrm{i(PR)}}$ is the PR integrated rain rate at each 4-km PR resolution cell, and N is the number of PR measurements within the SeaWinds footprint. Then, all antenna-weighted rain rates corresponding to each WVC are averaged, yielding the weighted average rain rate

$$R_{\mathrm{w}}^{\mathrm{wvc}} = \frac{1}{K} \sum_{k} R_{\mathrm{wk}} \tag{28}$$

where k indexes the K measurements in the WVC. An example 25×25 km WVC, the 6-dB contours of individual measurements comprising the WVC, and colocated 4-km PR rain rates are displayed in Fig. 1. To facilitate a comparison, WVC-average nonweighted rain rate estimates $R_{\mathrm{nw}}^{\mathrm{wvc}}$ are obtained by averaging all raw 4-km PR rain rates lying within each 25 km $\times$ 25 km WVC. Fig. 1 illustrates the large area covered by the measurements and the high variability of rain within the view of the large SeaWinds footprints.

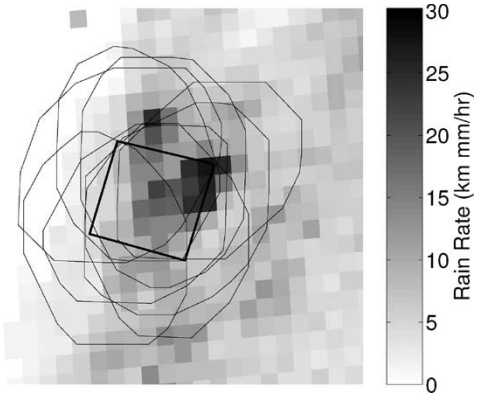

Fig. 1. Geometry of a sample WVC (bold square) and the 6-dB gain contours of the individual σ° measurements (ellipses) comprising the WVC. A PR-derived rain map is shown in the background.

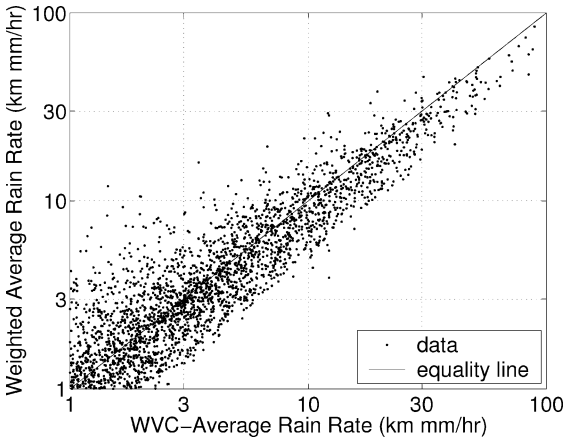

Fig. 2. WVC-average (unweighted) rain rate versus the weighted average rain rate seen by SeaWinds.

A scatter plot comparing the WVC-average rain rates to the weighted average rain rates for the colocated TRMM/SeaWinds dataset is displayed in Fig. 2. The statistics of the normalized error are calculated for all measurements with WVC-average rain rates greater than 2 km $\cdot$ mm/hr. The mean of the normalized error, defined as $\epsilon = (R_{\mathrm{w}}^{\mathrm{wvc}} - R_{\mathrm{nw}}^{\mathrm{wvc}})/R_{\mathrm{nw}}^{\mathrm{wvc}}$, for the colocated dataset is about -0.04, suggesting a slight negative bias of the weighted-average estimates. The standard deviation is 0.39, suggesting that the variability due to the WVC-filling effect is significant. Thus, it is important to interpret SeaWinds-derived rain rates as an irregularly weighted average of the rain, rather than an unweighted average of rain over the 25×25 km WVC.

V. Estimation of K_{pe}

In order to apply the MLE method to simultaneous wind/rain estimation, the normalized standard deviation of the effective rain backscatter K_{pe} must be determined. Several factors may

contribute to K_{pe} including, but not exclusive to, uncertainty in the model and intermeasurement variability due to nonuniform rain). We present estimated K_{pe} values due to both of these factors in Section V-A. Also, we present an empirical approach to estimating K_{pe} by finding the value of K_{pe} that yields the most accurate wind speeds in Section V-B. The empirical K_{pe} is used in the remainder of the paper.

A. K_{pe} Due to Model Uncertainty and Non-Uniform Rain

We first examine the rain backscatter model uncertainty. Validation of the wind/rain backscatter model [see (9)] given in [14] yields a normalized standard deviation due to uncertainty in the model of 1.6 dB, corresponding to a K_{pe} value of 0.45. This, however, may be an overestimate, augmented by the inherent variability of the NCEP winds and TRMM PR rain rates used to validate the model. Thus, we expect the actual variability to be lower than this estimate.

Second, we examine the intermeasurement variability of the rain backscatter within a WVC due to rain nonuniformity. The contribution to K_{pe} from intermeasurement variability due to rain nonuniformity is estimated using the colocated QuikSCAT/TRMM data by comparing the model backscatter computed from the weighted-average rain rate over the entire WVC to the model backscatter of the rain corresponding to individual measurements. The model estimate of the backscatter for the entire WVC, σ_e^{wvc}, is computed by projecting the weighted WVC-average rain rate $R_{\mathrm{w}}^{\mathrm{wvc}}$ through the rain model. Likewise, for all QuikSCAT measurements in the WVC, the model backscatter corresponding to each measurement σ_e is computed by forward projection of the antenna-weighted rain rate R_{w} through the rain model. An estimate of K_{pe} is obtained by taking the standard deviation of the normalized error

$$K_{pe} = \mathrm{std}\left\{\frac{(\sigma_e - \sigma_e^{\mathrm{wvc}})}{\sigma_e^{\mathrm{wvc}}}\right\} \tag{29}$$

for all rain rate observations where the weighted average rain rate is greater than 2 km · mm/h. The resulting value is $K_{pe} \cong 0.39$, indicating that intermeasurement variability is important and on the order of the model uncertainty.

B. K_{pe} Yielding Lowest RMS Wind Error

Since the value of K_{pe} affects the likelihood function, which in turn influences simultaneous wind/rain retrieval, an alternate approach to estimating K_{pe} is to find the value of K_{pe} that yields the best wind speed retrieval in real SeaWinds data. Here, we compare the retrieved wind speed from simultaneous wind/rain retrieval to NCEP wind speeds over the QuikSCAT/TRMM/NCEP colocated dataset.

In comparing QuikSCAT to NCEP, we note that a bias exists between nonraining QuikSCAT data and NCEP winds [7], [14]. This bias is partially due to differences in reference heights between the 10-m SeaWinds wind, and the 1000-mbar NCEP winds. We adjust for the bias with a multiplicative constant determined using least squares linear estimation over the nonraining QuikSCAT winds (as determined from the TRMM PR rain rate). The bias constant is determined to be $u_{\mathrm{qscat}} = 0.83 \times u_{\mathrm{ncep}}$. The remaining discussion uses NCEP wind speeds adjusted for the bias.

TABLE I
K_{pe} VALUE YIELDING THE LOWEST RMS WIND SPEED ERROR WHEN COMPARED WITH CALIBRATED NCEP NUMERICAL WEATHER PREDICTION WINDS OVER THE TRMM/QUIKSCAT COLOCATED DATASET. ALSO, THE CORRESPONDING RMS ERRORS FOR BOTH VARIANCE EQUATIONS

Variance form	K_{pe}	RMS wind speed error
Eq. (21)	0.18	2.27 m/s
Eq. (24)	0.16	2.14 m/s

TABLE II
DELINEATIONS OF WIND SPEED, WIND DIRECTION, RAIN RATE, AND CROSS-TRACK POSITION FOR WHICH THE SIMULATIONS ARE PERFORMED

Speed	3, 7, 11, 15, 20, 25 m/s
Direction	0°, 15°, 30°, ..., 345°
Rain Rate	0, 0.3, 1, 3, 10, 30 km mm/hr
Cross Track Position	WVC 2, 6, ... 38; 39, 43, ... 75

To find the value of K_{pe} that gives the best speed wind retrieval, we perform simultaneous wind and rain retrieval over the colocated TRMM/SeaWinds dataset for varying values of K_{pe} and for both likelihood function variance equations [(21) and (24)]. Then, we choose the value of K_{pe} and corresponding variance equation that yields the lowest root mean-square (rms) wind speed error overall. We note that we use the JPL default value of $K_{pm} = 0.16$ for the model function variability in the retrievals. The optimal values of K_{pe} for each variance equation and the rms error are given in Table I.

The optimal value of K_{pe} is 0.16 corresponding to the reduced variance form of (24). Since this value of K_{pe} is the same as the K_{pm} value used, the variance reduces to the nonraining variance equation [see (25)]. Thus, for the remaining analysis, we utilize the nonraining variance equation in the retrievals with $K_{pm} = 0.16$.

VI. SIMULATIONS AND VALIDATION

In order to evaluate the quality of the new wind/rain estimation procedure, we present a simulation and validation study for simultaneous wind/rain retrieval and rain-corrected wind retrieval. For SeaWinds baseline wind-only retrieval, it is known that for some wind speeds and cross-track positions, the wind retrieval performance of SeaWinds is somewhat degraded [24], [32]. This degradation often occurs at low and extremely high winds, at nadir, and on the swath edges. At low wind speeds, low SNR often causes wind estimates to be noisy. At high wind speeds, a saturation in σ° occurs, decreasing the accuracy of the winds [33], [34]. On the swath edges and at nadir, poor viewing geometry causes the MLE to be ill-conditioned. However, at moderate wind speeds, and especially in the "sweet spots" of the swath, wind retrieval performance is very good.

In the absence of rain, the inclusion of a rain rate parameter into the estimation process inherently makes the MLE more ill-conditioned than wind-only retrieval. However, when rain is present, simultaneous wind/rain retrieval can significantly improve the wind estimate. It is thus important to evaluate the performance of the wind/rain MLE procedure with and without rain. Also, because the wind retrieval accuracy varies with cross-track position and wind velocity, we evaluate the performance given a variety of cross-track and wind conditions. The MLE is evaluated via simulation in Section VI-A for both simultaneous

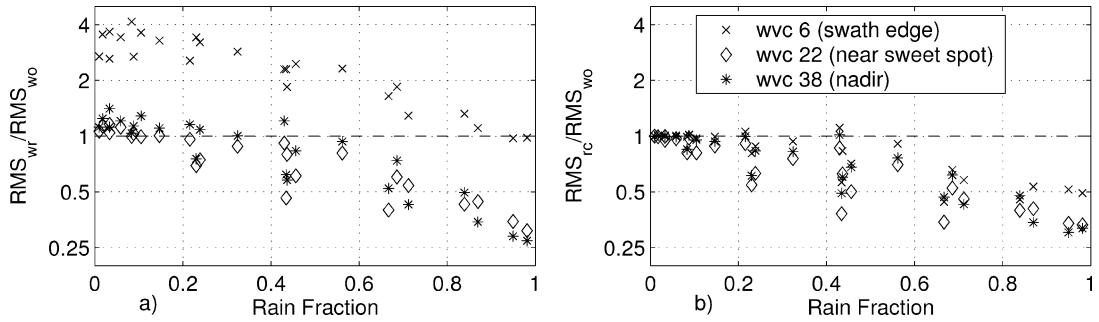

Fig. 3. Ratio of rms error between (a) the simultaneous wind/rain retrieval ($\mathrm{RMS_{wr}}$) and the wind-only retrieval ($\mathrm{RMS_{wo}}$) and (b) the rain-corrected wind retrieval ($\mathrm{RMS_{rc}}$) and the wind-only retrieval ($\mathrm{RMS_{wo}}$) as a function of rain fraction.

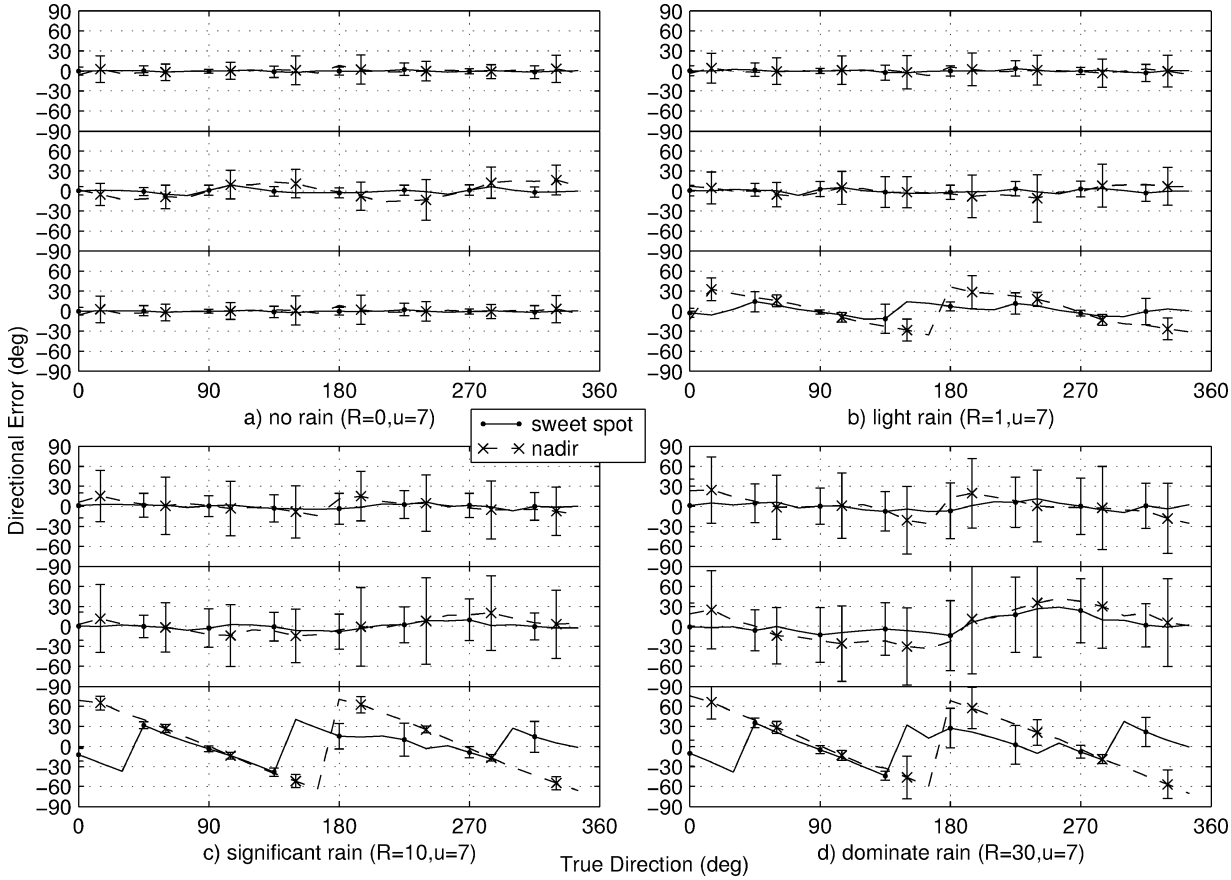

Fig. 4. Directional error statistics as a function of true direction for four rain rate cases with wind speed of 7 m/s. In each plot, the rain-corrected wind retrieval is shown on top, simultaneous wind/rain retrieval is in the middle, and wind-only retrieval is on the bottom.

wind/rain and rain corrected retrievals. Validation of simultaneous wind/rain retrieval with NCEP winds and PR rain rates is given in Section VI-B.

A. Simulation Results

To analyze the performance of the MLE, we perform simulations of the backscatter return for various conditions and evaluate the statistics of the retrieved wind and rain. Simulations are conducted for varying wind speeds, rain rates, wind directions, and cross-track positions, spanning a wide range of the parameter space (see Table II). Nominal values of the K_{pc} coefficients α, β, and γ are used with typical measurement geometries at each WVC.

For each combination of conditions, we project the speed, direction, and rain rate through the backscatter model [(9)] for all measurements corresponding to that WVC. Next, zero-mean Gaussian random noise with the variance given in (25) is added. Retrieval is then performed for 500 noise realizations for each set of conditions. The wind vector ambiguity realization that is closest to the true wind vector is selected.

For each simulation, three retrievals are performed: conventional wind-only retrieval, simultaneous wind/rain retrieval, and rain-corrected wind retrieval. In wind-only retrieval, the baseline wind-only likelihood function of (8) is used. In simultaneous wind/rain retrieval, ambiguities are determined as the local minima of the wind/rain likelihood function of (26). In rain-corrected retrieval, the simultaneous rain/wind likelihood function [see (26)] is evaluated at the true rain rate only, requiring knowledge of the true rain rate available from simulation.

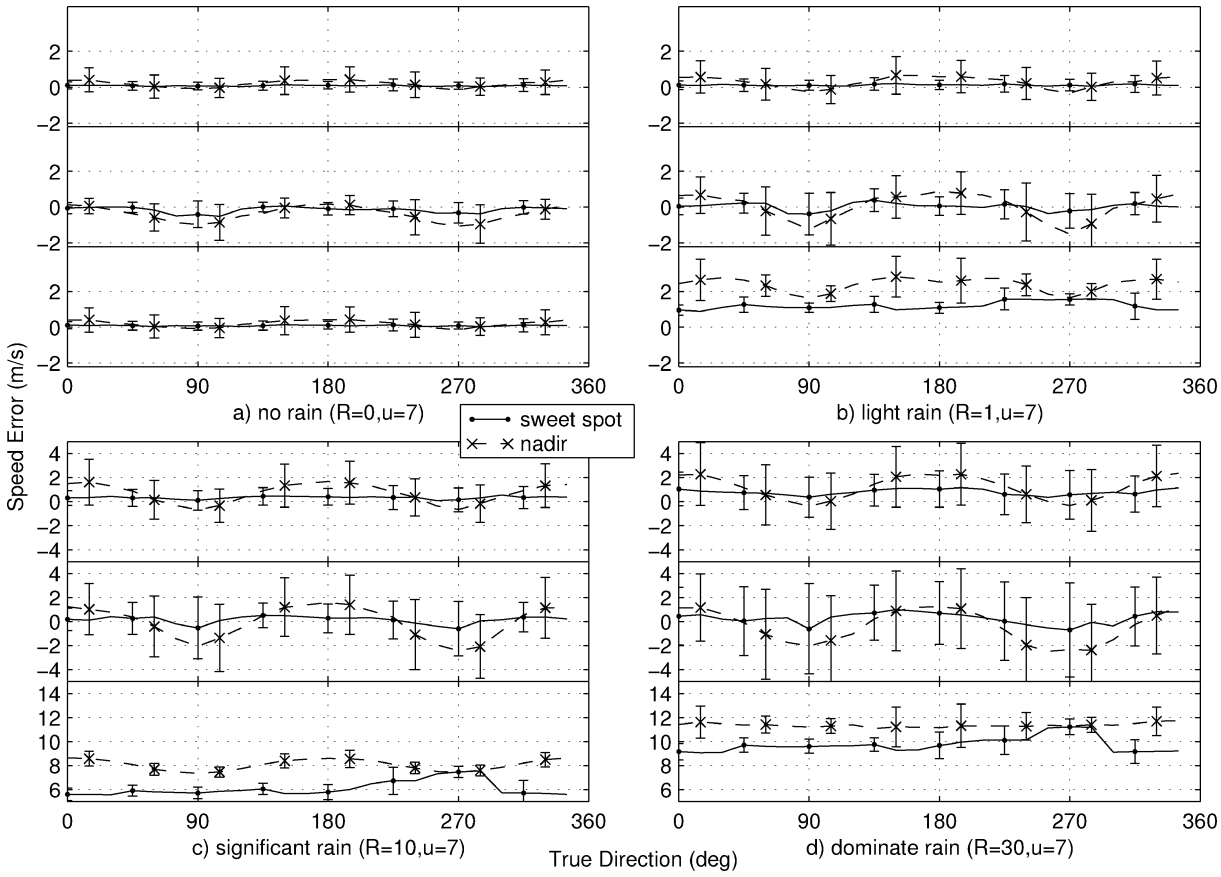

Fig. 5. Wind speed error statistics as a function of true direction for four rain rate cases with wind speed of 7 m/s. In each plot, the rain-corrected wind retrieval is shown on top, simultaneous wind/rain retrieval is in the middle, and wind-only retrieval is on the bottom. Notice the scale differences of the plots.

In presenting the simulation results, we first examine the rms error of the ambiguity closest to the true wind as a function of cross-track position and "rain fraction." The rain fraction F is defined as the effective rain backscatter divided by the total model backscatter given the ambiguity selected rain rate and vector wind averaged over the measurements

$$F = \sum_k \frac{\sigma_{ek}(R)}{\mathcal{M}_{rk}(R, \mathbf{u}, \ldots)}. \tag{30}$$

The rain fraction F indicates the level to which rain affects the backscatter measurements, with zero meaning rain has no significant effects and one meaning rain dominates the observed backscatter.

To allow compact comparison of wind-only retrieval to simultaneous wind/rain and rain-corrected retrievals, the ratio of the rms error between simultaneous and wind-only, and rain-corrected and wind-only is shown in Fig. 3 for three cross-track positions. Fig. 3(a) demonstrates that simultaneous wind/rain retrieval on the swath edge performs poorly as indicated by a high error ratio. Also from Fig. 3(a), simultaneous wind/rain retrieval is less accurate than wind-only retrieval for zero to low rain fraction data (corresponding to relatively low rain rates). However, for most rain fractions above 0.2, simultaneous rain/wind retrieval has a lower rms error, especially for sweet-spot observations. These simulations suggest that simultaneous wind/rain retrieval works well for most rain corrupted cases, while it slightly degrades wind retrieval performance in zero-rain conditions. The degradation in rain-free conditions occurs because the simultaneous wind/rain retrieval introduces a third free parameter (rain) into the estimation process. It is thus possible to spuriously retrieve rain in such situations, especially where the wind backscatter response is similar to a rain signature. In such conditions, the retrieved wind is less accurate. This problem is examined further in the companion paper [20].

Comparing Fig. 3(b) to 3(a), the rain-corrected wind retrieval performs better than the wind-only retrieval for almost all cases except at high rain fractions, where the wind is almost totally dominated by rain. The most noticeable improvement over simultaneous wind/rain retrieval is on the swath edges, where simultaneous wind/rain retrieval does poorly. Also, as expected, the rain-corrected wind retrieval performs much the same as wind-only retrieval in zero- and low rain cases.

Next, we examine the directional and speed error of the two retrieval methods, comparing them to the wind-only result. The high number of wind/rain/direction/cross-track combinations prohibits displaying all the cases in this paper. Thus, we only show several representative examples. Since 7 m/s is the mean wind speed over the oceans, we show four typical cases with wind speed of 7 m/s and varying rain rates. For clarity, we show nadir and sweet spot simulations only. Figs. 4 and 5 show the directional and speed error statistics for rain rates of 0, 1, 10, and 30 km $\cdot$ mm/h for rain-corrected retrieval, simultaneous wind/rain retrieval, and wind-only retrieval. For the zero-rain

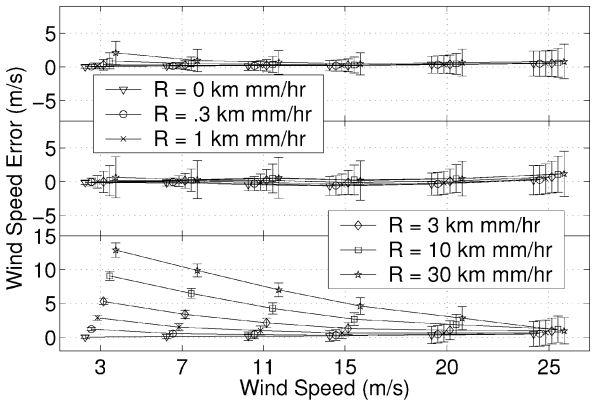

Fig. 6. Wind speed error statistics, showing (line) the mean bias and (error bars) standard deviation, as a function of wind speed for various rain rates. (Top) The rain-corrected wind retrieval. (Middle) Simultaneous wind/rain retrieval. (Bottom) Wind-only retrieval. Points are horizontally offset for clarity.

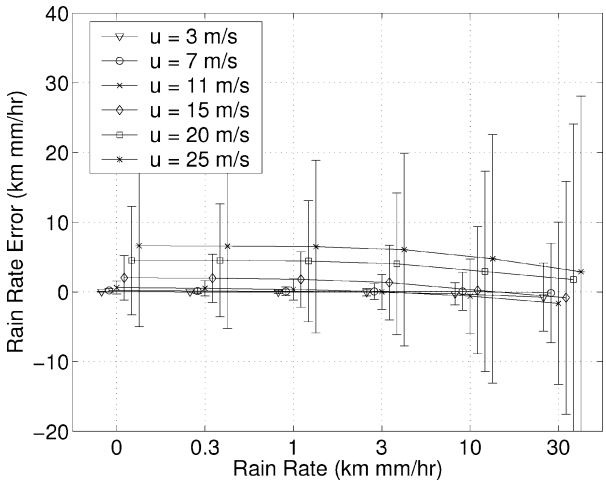

Fig. 7. Rain rate error statistics, showing (line) the mean bias and (error bars) standard deviation, as a function of rain rate for several different wind speeds. Points are horizontally offset for clarity.

case, the simultaneous wind/rain retrieval of directions is somewhat less accurate than the other two retrieval methods. However, for light rain, simultaneous wind/rain retrieval is more accurate, while wind-only retrieval becomes somewhat biased. For significant rain, the rain-corrected and simultaneous wind/rain retrieval are very close to zero-mean, while the wind-only retrieval is extremely biased in certain directions. The bias in the wind-only data exists because the wind-only ambiguities tend to point in a direction parallel or perpendicular to the swath, regardless of the true direction. For the dominant rain case, all three retrievals perform poorly with respect to wind direction, as expected; however, the rain-corrected and simultaneous wind/rain retrievals are less biased. Figs. 4 and 5 also demonstrate that simultaneous wind/rain directional retrieval has a lower variance in the sweet spot than in the nadir region. Thus, directional retrieval in the sweet spot is somewhat better than at nadir.

Examining the speed error statistics of Fig. 5, the simultaneous wind/rain retrieved wind speeds are nearly zero mean for all rain rates with increasing variability at high rain rates, while the wind speeds for the wind-only retrieval are extremely biased at high rain rates. At high rain rates, the simultaneous wind/rain retrieved speed is biased slightly low for directions nearing 90° and 270°, especially at nadir. The bias is likely due to cross-track pointing winds appearing to the MLE as rain and, thus, decreasing the wind speed while increasing the rain rate. This bias suggests identifiability problems between the wind and rain for cross-track blowing winds (see [20]).

The speed error for the three retrieval methods is further demonstrated in Fig. 6. Here, all simulation wind speed and rain rate combinations are shown. As expected, the wind-only retrieval shows considerable biases at low wind speeds for moderate to high rain rates. These biases are almost completely corrected in both rain-corrected and simultaneous wind/rain retrieval, which both exhibit a near-zero mean for almost all cases. The rain-corrected retrieval is slightly biased high for very low rain rates and high wind speeds. Likewise, the simultaneous wind/rain retrieved speeds are slightly biased high for most rain rate/wind speed combinations.

Next, we demonstrate the rain retrieval performance of the simultaneous wind/rain MLE. Fig. 7 shows the rain rate error statistics of the retrieved rain rates as a function of true rain rate for varying wind speeds. As wind speed increases, the retrieved rain rate becomes increasingly biased. The rain rate bias at high wind speeds is quite high, even at zero rain rate. However, in low to moderate wind speeds (3–11 m/s), the retrieval performs quite well. These simulations demonstrate the limitation of accurately retrieving rain in high wind speed regions where the wind dominates the rain signal. Rain flagging algorithms can be developed to detect erroneous rain rates in high wind speed regions and discard them (see [20]).

In summary, simultaneous wind and rain retrieval works well for many conditions, especially in the sweet spot and for moderate wind/rain conditions. Nadir-retrieved winds from the simultaneous method tend to be especially noisier than winds retrieved in the sweet spots, and simultaneous wind/rain retrieval is not usable on the swath edges. In the absence of rain, simultaneous wind/rain retrieval is less accurate than wind-only retrieval, and thus, it is beneficial to use wind-only retrieval in nonraining regions. The wind speeds of simultaneous wind/rain retrieval are mostly unbiased; however, cross-track blowing winds may cause lower than expected retrieved wind speeds due to increased ambiguity between the wind and rain effects in such conditions. Also, in extreme wind, the retrieved rain rate tends to be biased high, while in extreme rain, the retrieved wind vectors tend to be highly variable.

B. Validation

In this section, we present a validation of QuikSCAT simultaneous wind/rain retrieval with NCEP wind speeds/directions in Section VI-B1, and with TRMM PR rain rates in Section VI-B2. The validation of rain-corrected wind retrieval is reserved for a future paper. Also, as of yet, AMSR rain rate estimates are not available to use in conjunction with rain-corrected wind retrieval. We note that the "wind-only" retrieval referenced here is the JPL baseline ambiguity selected winds (with thresholded

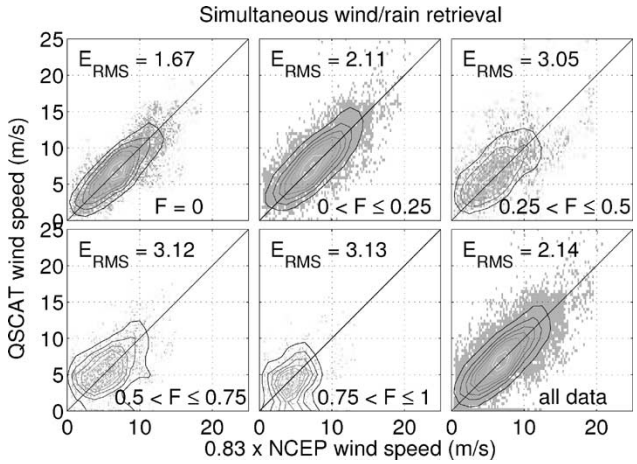

Fig. 8. Scatter plot with density curves of the bias-corrected NCEP wind speeds versus simultaneous wind/rain-retrieved wind speeds for various rain fraction bins.

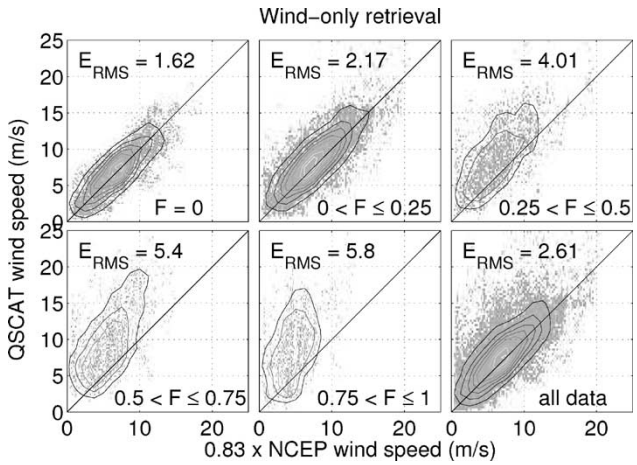

Fig. 9. Scatter plot with density curves of the bias-corrected NCEP wind speeds versus wind-only retrieved wind speeds for various rain fraction bins.

nudging, but without direction interval retrieval; see [27]). We also note that we omit the swath edges from the comparison.

1) Wind Vector Validation: First, we perform validation of simultaneous wind/rain retrieval with NCEP wind speeds and directions. The validation is performed over the colocated QuikSCAT/TRMM dataset. We correct for the NCEP bias with a multiplicative constant of 0.83.

A scatter plot displaying the simultaneous wind/rain retrieved and wind-only retrieved wind speed as a function of NCEP wind speed for several rain fraction bins is shown in Figs. 8 and 9. Simultaneous wind/rain retrieval has a slightly higher error than the wind-only retrieval for low rain fractions. However, for increasing rain fractions, the simultaneous wind/rain retrieval remains essentially unbiased, while the wind-only retrieval becomes increasingly biased.

At higher rain fractions, many of the wind speed estimates from simultaneous wind/rain retrieval are driven to zero. A "zero" wind speed indicates that either the rain is sufficiently strong so that it totally dominates the signal, or that the backscatter from the wind appears to the MLE as rain. These spurious zero wind speeds occur in about 0.02% of rain-free data, 0.12% of data with rain fractions between 0 and 0.25,

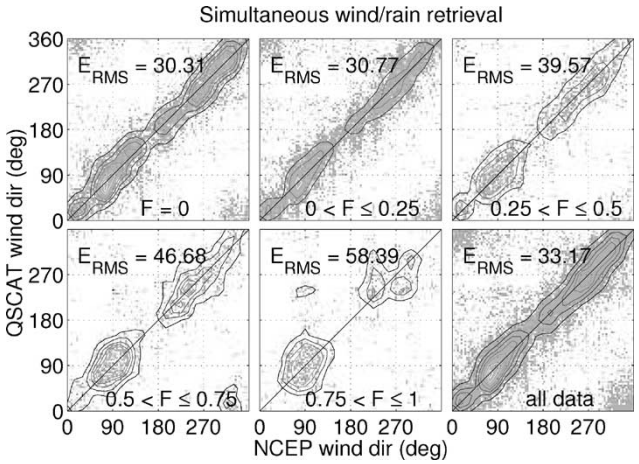

Fig. 10. Scatter plot with density curves of NCEP wind directions versus simultaneous wind/rain retrieved wind directions for various rain fraction bins.

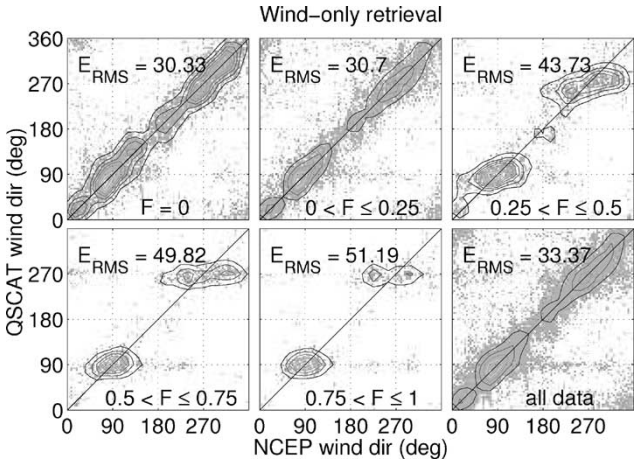

Fig. 11. Scatter plot with density curves of NCEP wind directions versus wind-only retrieved wind directions for various rain fraction bins.

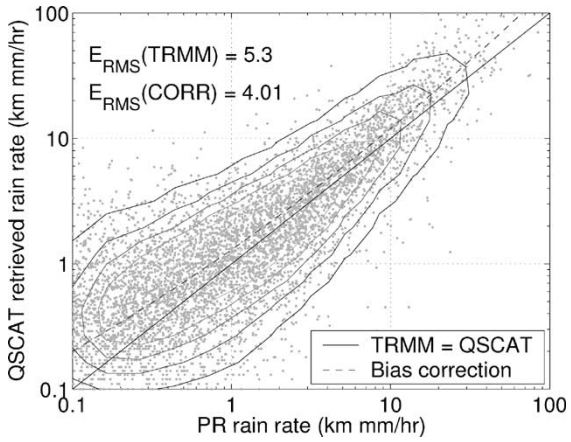

Fig. 12. Scatter plot of TRMM PR-derived "effective" weighted average rain rates versus QuikSCAT-derived rain rates. Density curves are shown, along with (solid line) the equality line. (Dotted line) Best quadratic fit to TRMM rain rate (in log space).

3% of data with rain fractions between 0.25 and 0.5, 8% of data with rain fractions between 0.5 and 0.75, and 19% of data with rain fractions above 75%. Thus, the zero wind speed occurrences are mainly in areas of significant rain.

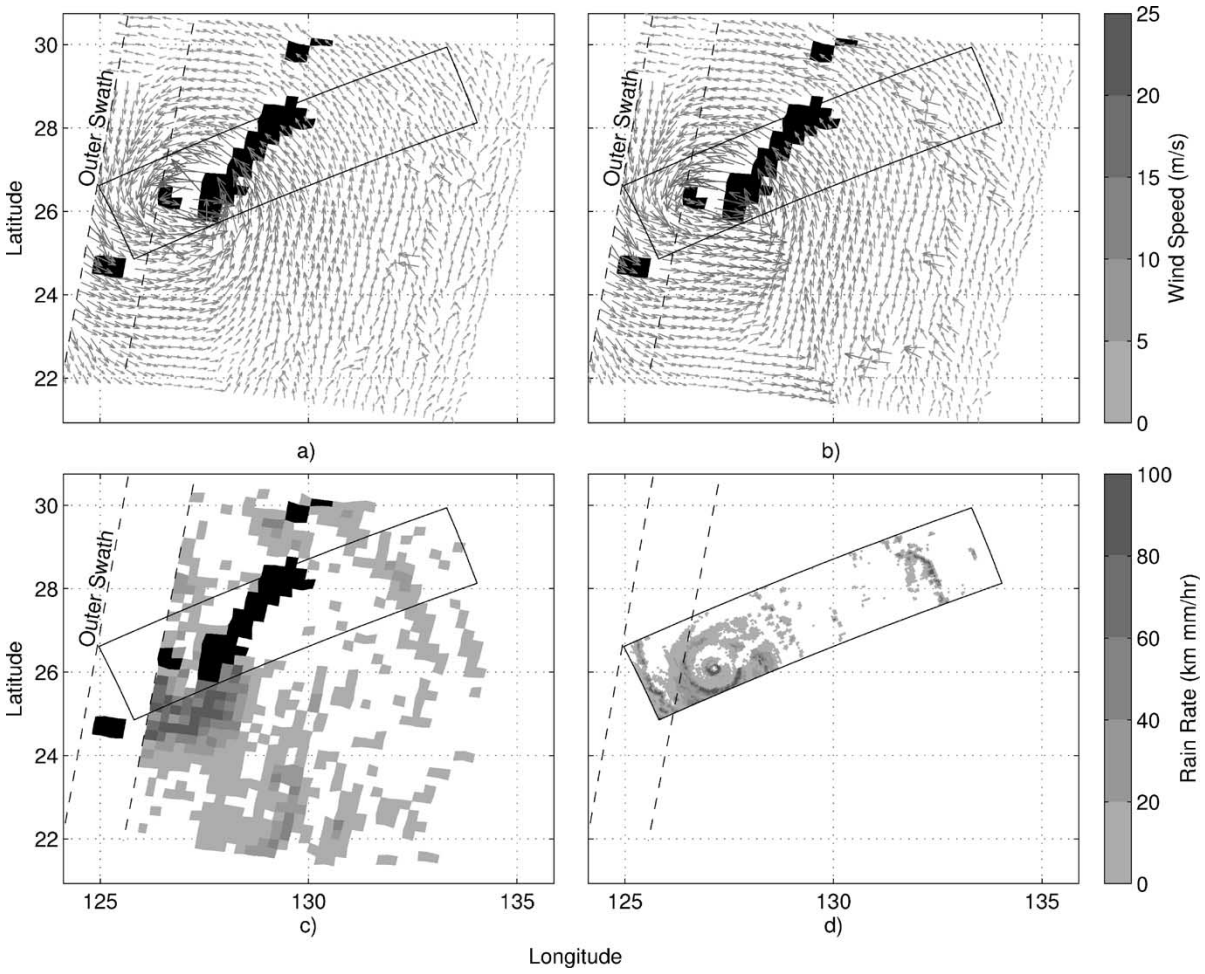

Fig. 13. Synoptic example of a hurricane. (a) QuikSCAT simultaneous wind/rain derived wind vectors. (b) QuikSCAT wind-only retrieval. (c) QuikSCAT simultaneous wind/rain derived rain rates. (d) Raw PR rain rates. The box shows the coverage of the PR data. Black pixels represent WVCs flagged as containing land.

Validation of directional retrieval is demonstrated in Figs. 10 and 11. We note that we have excluded data that have zero wind speed in the simultaneous wind/rain retrieval from the analysis in both wind-only and simultaneous/wind rain datasets, because the simultaneous wind/rain direction is undefined in such situations. At higher rain fractions, the simultaneous wind/rain directions are much closer to the true directions, while at rain fractions above 0.25, the wind-only retrieval begins to have retrieved directions at only 90° and 270° (cross swath). Thus, where rain is significant, simultaneous retrieval aids in correcting wind directions corrupted by rain. The exception is at very high rain fractions > 0.75, where the rain dominates and neither wind-only or simultaneous wind/rain retrieval are valid.

The rms directional error of the selected ambiguities for rain-free data is around 30% for both cases, which is higher than expected. This is partially due to the fact that the dataset covers mainly areas containing significant patches of rain, where ambiguity selection is generally poor [32]. Another contributor to the higher error is the fact that we have included low wind speeds (< 4 m/s) in the analysis, which are generally noisier than moderate wind speeds (> 4 m/s). Excluding data below 4 m/s reduces the wind-only rms directional error to 24° in rain-free conditions, and the simultaneous wind/rain directional error to 25° in rain-free conditions. However, removing the low wind speed data decreases the overall rms directional error to 27° for wind-only retrieval, while it decreases the rms directional error only to 29° for simultaneous retrieval. Thus, while the wind directions for simultaneous wind/rain retrieval are less biased, they have increased variability.

2) Rain Rate Validation: Next, we compare the QuikSCAT-retrieved rain rates to the PR-derived weighted average rain rates over the colocated dataset. A scatter plot of PR rain rates against QuikSCAT rain rates is shown in Fig. 12. Since the plot is on a log-log scale, rain rates less than 0.1 km · mm/h (the zero-rain cases) in either of the QuikSCAT or TRMM PR datasets are not displayed. Of the rain rates that are zero in one of the two datasets, the vast majority (about 93%) have relatively small rain rate values (< 2 km · mm/h) in the other dataset.

Although the QuikSCAT derived rain rates have considerable scatter in comparison to the PR rain rates, Fig. 12 demonstrates a strong correlation between QuikSCAT and PR-derived rain rates. The QuikSCAT rain rates are biased somewhat high, which is expected from the simulation. However, the bias can be corrected. For example, Fig. 12 shows a quadratic fit of the QuikSCAT rain rates to the TRMM rain rates that can be used

to correct for the bias. The bias correction reduces the rms error by about a fourth. Using the bias correction, the rain backscatter model could be tuned to yield an unbiased estimate.

VII. Synoptic Example

In this section, we examine a colocated PR/QuikSCAT example over a hurricane. The location of the storm is over the Ryukyu Islands off the southern tip of Japan on September 22, 1999. Fig. 13 shows the QuikSCAT-derived wind vectors for both simultaneous wind/rain and wind-only retrieval, along with the QuikSCAT-derived rain rates and the colocated TRMM PR derived rain rates.

On the far left, the coverage of the storm is limited to the outer-beam region of the QuikSCAT swath. Retrieval of rain in this area is not usable. Thus, wind-only vectors are used in the outer swath region of Fig. 13(a).

The wind-only retrieval exhibits many rain-induced features that are corrected by the simultaneous wind/rain retrieval. The most obvious of these features are the rain bands located up to about 24 wind vector cells (600 km) from the center of the storm. The rain band is also visible in the TRMM PR data. The wind-only retrieval shows dramatic "apparent" wind speed increases and corrupted directions in the rain band due to the electromagnetic scattering from rain. The simultaneous wind/rain retrieval yields wind speeds in the rain bands that are more consistent with the wind speeds of neighboring WVCs, along with generally more self-consistent directions.

Another rain feature corrected by simultaneous wind/rain retrieval is the wind corruption due to the large area of rain just south of the storm center. In this case, the wind-only retrieval shows wind vectors all pointing in the cross-track direction (nearly east), an indicator of rain. The QuikSCAT-retrieved rain rates are very high in this region, consistent with the TRMM retrieved rains compared to the portion covered by the PR. The simultaneous wind/rain retrieval shows a much more consistent circular flow in this region, suggesting better wind retrieval over the wind-only method. These corrected features demonstrate that simultaneous wind/rain retrieval has the capability of correcting rain-corrupted winds.

VIII. Conclusion

QuikSCAT is a spaceborne scatterometer, originally designed to measure ocean winds. Rain has been shown to be one of the most significant factors that corrupts wind scatterometer data. The new technique of simultaneously retrieving ocean winds and rain significantly improves the wind speed estimate for many rain-corrupted areas. As a side benefit, simultaneous wind/rain retrieval provides an estimate of the rain rate, which, while somewhat noisy and biased, has broad coverage and can complement instruments such as the TRMM PR. When an outside estimate of the rain rate is available, rain-corrected wind retrieval can be used to further improve the rain/wind estimates.

SeaWinds on QuikSCAT rain retrieval has been shown by simulation to give the best results in the swath sweet spot and perform with reduced accuracy on the swath edges (the outer nine WVCs on either side of the swath). Simulation also demonstrates that wind speeds from simultaneous wind/rain retrieval are nearly unbiased, while the wind-only retrieval produces increasingly biased estimates as rain increases. However, in zero-rain conditions, the inclusion of the rain rate parameter into the retrieval process can give rise to spurious rain rate estimates and correspondingly lower wind retrieval accuracy at those WVCs. It is thus most beneficial to perform simultaneous retrieval only in raining areas.

The rain-corrected wind retrieval method presented in this paper enables synergistic use of the SeaWinds scatterometer with radiometer data such as was planned with the AMSR aboard ADEOS II before the spacecraft's failure in late October 2003. However, similar methods can be used with future scatterometer missions. In addition, the simultaneous wind/rain method can be applied for reanalysis of SeaWinds on QuikSCAT data to improve the wind vector estimates and to provide an auxiliary dataset of worldwide rain rates.

References

[1] M. W. Spencer, C. Wu, and D. G. Long, "Tradeoffs in the design of a spaceborne scanning pencil beam scatterometer: Application to SeaWinds," *IEEE Trans. Geosci. Remote Sensing*, vol. 35, pp. 115–126, Jan. 1997.

[2] A. Bentamy, E. Autret, P. Queffeulou, and Y. Quilfen, "Intercomparison of ERS-2 and QuikSCAT winds," in *Proc. IGARSS*, vol. 1, Honolulu, HI, 2000, pp. 234–236.

[3] P. Queffeulou and A. Bentamy, "Comparison between QuikSCAT and altimeter wind speed measurements," in *Proc. IGARSS.*, vol. 1, 2000, pp. 269–271.

[4] R. K. Moore and A. D. Fung, "Radar determination of winds at sea," *Proc. IEEE*, vol. 67, pp. 1504–1521, 1979.

[5] F. T. Ulaby, R. K. Moore, and A. K. Fung, *Microwave Remote Sensing Active and Passive*. Norwood, MA: Artech House, 1981.

[6] F. J. Wentz and D. K. Smith, "A model function for the ocean-normalized radar cross section at 14 GHz derived from NSCAT observations," *J. Geophys. Res.*, vol. 104, no. C5, pp. 11 499–11 514, May 1999.

[7] F. J. Wentz, M. H. Freilich, and D. K. Smith, "NSCAT-2 geophysical model function," in *Proc. 1998 Fall AGU Meeting*, 1998.

[8] M. H. Freilich and R. S. Dunbar, "Derivation of satellite wind model functions using operational surface wind analyses—An altimeter example," *J. Geophys. Res.*, vol. 98, no. C8, pp. 14 633–14 649, Aug. 1993.

[9] C. Chi and F. K. Li, "Comparative study of several wind estimation algorithms for spaceborne scatterometers," *IEEE Trans. Geosci. Remote Sensing*, vol. 26, pp. 115–121, Mar. 1988.

[10] R. K. Moore, A. H. Chaudhry, and I. J. Birrer, "Errors in scatterometer-radiometer wind measurement due to rain," *IEEE J. Oceanic Eng.*, vol. 8, pp. 37–48, Jan. 1983.

[11] L. F. Bliven and J. P. Giovanangeli, "Experimental study of microwave scattering from rain- and wind-roughened seas," *Int. J. Remote Sens.*, vol. 14, pp. 855–869, 1993.

[12] L. F. Bliven, P. W. Sobieski, and C. Craeye, "Rain generated ring-waves: Measurements and modeling for remote sensing," *Int. J. Remote Sens.*, vol. 18, no. 1, pp. 221–228, 1997.

[13] D. E. Weissman, M. A. Bourassa, and J. Tongue, "Effects of rain rate and wind magnitude on SeaWinds scatterometer wind speed errors," *J. Atmos. Ocean. Tech.*, vol. 19, no. 5, pp. 738–746, May 2002.

[14] D. W. Draper and D. G. Long, "Evaluating the effect of rain on SeaWinds scatterometer measurements," *J. Geophys. Res.*, no. C12, 2004. DOI: 10.1029/2002JC001741.

[15] J. N. Huddleston and B. W. Stiles, "A multi-dimensional histogram rain flagging technique for SeaWinds on QuikSCAT," in *Proc. IGARSS.*, vol. 3, Honolulu, HI, 2000, pp. 1232–1234.

[16] C. A. Mears, D. Smith, and F. J. Wentz, "Detecting rain with QuikSCAT," in *Proc. IGARSS*, Honolulu, HI, 2000, pp. 1235–1237.

[17] M. Portabella and A. Stoffelen, "Rain detection and quality control of SeaWinds," *J. Atmos. Oceanic Tech.*, vol. 18, no. 7, pp. 1171–1183, 2001.

[18] L. N. Connor, P. S. Chang, and J. R. Carswell, "Identification and possible correction of rain contamination in QuikSCAT/SeaWinds wind retrievals," in *Proc. IGARSS*, vol. 3, Honolulu, HI, 2000, pp. 1238–1240.

[19] W. L. Jones, K. Ahmad, J. Park, T. Kasparis, and J. Zec, "Validation of QuikSCAT radiometer rain rates using the TRMM microwave radiometer," in *Proc. IGARSS*, vol. 3, Toronto, ON, Canada, 2002, pp. 1816–1818.

[20] D. W. Draper and D. G. Long, "Assessing the quality of SeaWinds rain measurements," *IEEE Trans. Geosci. Remote Sensing*, vol. 42, pp. 1424–1432, July 2004.

[21] I. S. F. Jones and Y. Toba, *Wind Stress Over the Ocean*. Cambridge, U.K.: Cambridge Univ. Press, 2001.

[22] I. R. Young, *Wind Generated Ocean Waves*. Amsterdam, The Netherlands: Elseivier, 1999.

[23] F. M. Naderi, M. H. Freilich, and D. G. Long, "Spaceborne radar measurement of wind velocity over the ocean—An overview of the NSCAT scatterometer system," *Proc. IEEE*, vol. 79, pp. 850–866, June 1991.

[24] T. E. Oliphant and D. G. Long, "Accuracy of scatterometer derived winds using the Cramér-Rao bound," *IEEE Trans. Geosci. Remote Sensing*, vol. 37, pp. 2642–2652, Nov. 1999.

[25] JPL, "QuikSCAT Science data product user's manual," California Inst. Technol., Jet Propulsion Lab., Pasadena, CA, Tech. Rep. D-18 053, 2001.

[26] D. G. Long and M. W. Spencer, "Radar backscatter measurement accuracy for a spaceborne pencil-beam wind scatterometer with transmit modulation," *IEEE Trans. Geosci. Remote Sensing*, vol. 35, pp. 102–114, Jan. 1997.

[27] B. W. Stiles, B. D. Pollard, and R. S. Dunbar, "Direction interval retrieval with thresholded nudging: A method for improving the accuracy of QuikSCAT winds," *IEEE Trans. Geosci. Remote Sensing*, vol. 40, pp. 79–89, Jan. 2002.

[28] S. J. Shaffer, R. S. Dunbar, S. V. Hsiao, and D. G. Long, "A median-filter-based ambiguity removal algorithm for NSCAT," *IEEE Trans. Geosci. Remote Sensing*, vol. 29, pp. 167–174, Jan. 1991.

[29] B. W. Stiles and S. Yueh, "Impact of rain on spaceborne Ku-band wind scatterometer data," *IEEE Trans. Geosci. Remote Sensing*, vol. 40, pp. 1973–1983, Sept 2002.

[30] M. W. Spencer and M. Shimada, "Effect of rain on Ku-band scatterometer wind measurements," in *Proc. IGARSS*, vol. 3, 1991, pp. 1285–1288.

[31] D. W. Draper, "Wind scatterometry with improved ambiguity selection and rain modeling," Ph.D. dissertation, Brigham Young Univ., Provo, UT, 2003.

[32] D. W. Draper and D. G. Long, "An assessment of SeaWinds on QuikSCAT wind retrieval," *J. Geophys. Res.*, vol. 107, no. C12, pp. (5)1–(5)14, Dec. 2002.

[33] W. J. Donnelly, J. R. Carswell, R. E. McIntosh, P. S. Chang, J. Wilkerson, F. Marks, and P. G. Black, "Revised ocean backscatter models at C and Ku band under high-wind conditions," *J. Geophys. Res.*, vol. 104, pp. 11 485–11 497, 1999.

[34] L. Zeng and R. A. Brown, "Scatterometer observations at high wind speeds," *J. Appl. Meteorol.*, vol. 37, pp. 1412–1420, 1998.

David W. Draper received the Ph.D. degree in electrical engineering from Brigham Young University (BYU), Provo, UT, in 2003. His Ph.D. research included remote sensing of ocean winds and rain using satellite scatterometer data.

He is currently a Systems Engineer with Ball Aerospace, Boulder, CO. In 1999, he joined the Microwave Earth Remote Sensing research group, BYU. He has developed algorithms to identify typical errors in scatterometer wind estimation and is using wind and rain models to improve the wind estimation technique.

Dr. Draper is a Tau Beta Pi Fellow (2000–2001).

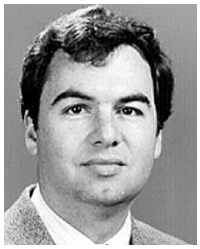

David G. Long (S'80–SM'98) received the Ph.D. degree in electrical engineering from the University of Southern California, Los Angeles, in 1989.

From 1983 to 1990, he was with the National Aeronautics and Space Administration (NASA) Jet Propulsion Laboratory (JPL), Pasadena, CA, where he developed advanced radar remote sensing systems. While at JPL, he was the Senior Project Engineer on the NASA Scatterometer (NSCAT) project, which was flown aboard the Japanese Advanced Earth Observing System (ADEOS) from 1996 to 1997. He was also the Experiment Manager and Project Engineer for the SCANSCAT scatterometer (now known as SeaWinds). In 1990, he joined the Department of Electrical and Computer Engineering, Brigham Young University (BYU), Provo, UT, where he currently teaches upper division and graduate courses in communications, microwave remote sensing, radar, and signal processing, is the Director of BYU's Center for Remote Sensing, and is the Head of the Microwave Earth Remote Sensing Laboratory. He is the Principal Investigator on several NASA-sponsored interdisciplinary research projects in microwave remote sensing and innovative radar systems. He has numerous publications in signal processing and radar scatterometry. His research interests include microwave remote sensing, radar, polar ice, signal processing, estimation theory, and mesoscale atmospheric dynamics. He has over 250 publications in the open literature.

Dr. Long has received the NASA Certificate of Recognition several times.